Adiabatic and nonadiabatic bond cleavages in Norrish type I reactions

ARTICLE · JANUARY 2011

READS
13

3 AUTHORS:

Ganglong Cui
Beijing Normal University
46 PUBLICATIONS **332** CITATIONS
SEE PROFILE

Zhigang Sun
Dalian Institute of Chemical Physics
72 PUBLICATIONS **1,059** CITATIONS
SEE PROFILE

Wei-Hai Fang
Beijing Normal University
233 PUBLICATIONS **4,481** CITATIONS
SEE PROFILE

THE JOURNAL OF PHYSICAL CHEMISTRY A

ARTICLE

pubs.acs.org/JPCA

Adiabatic and Nonadiabatic Bond Cleavages in Norrish Type I Reaction

Ganglong Cui,[†] Zhigang Sun,[‡] and Weihai Fang[†,*]

[†]Chemistry College, Beijing Normal University, Beijing 100875, People's Republic of China

[‡]State Key Laboratory of Molecular Reaction Dynamics and Center for Theoretical and Computational Chemistry, Dalian Institute of Chemical Physics, Chinese Academy of Sciences, Dalian 116023, People's Republic of China

Supporting Information

ABSTRACT: One of the fundamental photoreactions for ketones is Norrish type I reaction, which has been extensively studied both experimentally and theoretically. Its α bond-cleavage mechanisms are usually explained in an adiabatic picture based on the involved excited-state potential energy surfaces, but scarcely investigated in terms of a nonadiabatic picture. In this work, the S_1 α bond-cleavage reactions of $CH_3OC(O)Cl$ have been investigated by using the CASSCF and MRCI-SD calculations, and the ab initio based time-dependent quantum wavepacket simulation. The numerical results indicate that the photoinduced dissociation dynamics of $CH_3OC(O)Cl$ could exhibit strong nonadiabatic bond-fission characteristics for the S_1 α C−Cl bond cleavage, while the dynamics of the S_1 α C−O bond cleavage is mainly of adiabatic characteristics. This nonadiabatic mechanism for Norrish type I reaction of $CH_3OC(O)Cl$ is uncovered for the first time. The quantum wavepacket dynamics, based on the reduced-dimensional coupled potential energy surfaces, to some extent illustrates the significance of the nonadiabatic effect in the transition-state region on the dynamics of Norrish type I reaction.

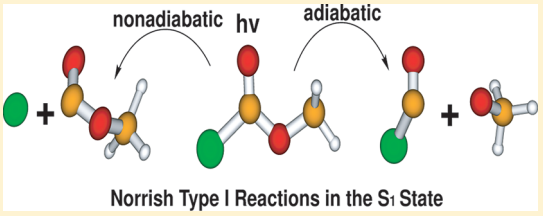

INTRODUCTION

The study of nonadiabatic effects in chemical reaction dynamics is one of the most current and active areas of investigation, where the validity of the Born−Oppenheimer approximation is challenged and reconsidered.[1−14] On the basis of this fundamental approximation, one usually predicts the branching between energetically allowed product channels using the statistical transition-state theories, which rely on a single adiabatic potential energy surface. This potential energy surface can give the energetic barriers for the involved reaction channels, based on which one can accurately calculate the reaction rate of each channel and thereby predict their branching. Nevertheless, the adiabatic approximation will fail in certain regions of potential energy surfaces where the nonadiabatic coupling between the pertinent electronic states is rather strong, for example near the transition states of photochemical reactions from which one molecule can nonadiabatically access both the upper and lower adiabatic electronic state or only the lower adiabatic electronic state.[1,2,4] For this reason, the inclusion of nonadiabatic effects to calculate the reaction rates and to predict the branching is very important, even necessary in certain regions of potential energy surfaces. However, before the calculations of rate constants and kinetics, we have to identify the strong nonadiabatic coupling regions of a multidimensional reactive potential energy surface by means of the high-level electronic structure methods.

Norrish type I reactions are conventionally defined as follows: the photochemical cleavage or homolysis of carbonyl compounds (aldehydes, ketones, and so forth) into two free radical intermediates.

$$RCOR' + h\nu \rightarrow RCO^{\bullet} + R'^{\bullet} \quad (1)$$

These intermediates can be formed either from singlet states or from triplet states as a result of intersystem crossing. This reaction is named after Norrish who first and experimentally explored these kinds of photochemical reactions in 1936.[15−18] Since then, Norrish type I reactions have attracted much attention both experimentally and theoretically.[17,19−28] Its α bond-fission mechanisms and the relevant calculations of rate constants, branching, and kinetics are in general explored and discussed using an adiabatic multidimensional potential energy surface. Nevertheless, this adiabatic bond-fission picture is invalid in certain regions of potential energy surfaces where the nonadiabatic coupling is strong, for example, in the transition-state regions.[2,4,6,29−32]

On the basis of the previous studies, the low-excitation-energy photodissociation mechanisms of the asymmetrically substituted aliphatic carbonyl compounds, $XC(O)Y$ (X, CH_3 and CH_3CH_2; Y, Cl, H, OH, and NH_2), can be grouped into three types with respect to the α bond fission.[24,33] The exclusive α bond cleavage in the S_1 state is one type, which frequently takes place in the

Received: June 6, 2011
Revised: August 7, 2011
Published: August 08, 2011

dx.doi.org/10.1021/jp2053025 | J. Phys. Chem. A 2011, 115, 10146–10153

acetyl halides (X, CH_3 and CH_3CH_2; Y, Cl, Br, and I).[34,35] The second type comprises acetone, acetaldehyde, and acetamide (X, CH_3; Y, CH_3, H, and NH_2) where the α bond fissions mainly occur in the T_1 state via the $S_1 \rightarrow T_1$ intersystem crossing (ISC).[26,27,36] Finally, in acetic acid (X, CH_3; Y, OH), there are two comparable dissociation channels: the S_1 direct α bond cleavage and the T_1 channel after the $S_1 \rightarrow T_1$ ISC.[25] Additionally, recently we have also studied the photodissociation dynamics of ester (X, CH_3O; Y, H) and proposed that its α bond cleavages are the special Norrish type I reactions. In $CH_3OC(O)H$, the S_1 state adiabatically correlates with the ground-state products of the α C−O bond fission, unlike the S_1 α C−H bond fission, which correlates with the excited-state products.[23,33,34] For the same bond fission, the height of the ground-state barrier is usually lower than that of the excited-state barrier. Hence, the S_1 direct C−O bond cleavage of $CH_3OC(O)H$ becomes the dominant channel with the low excitation energy.[23]

In contrast to $CH_3OC(O)H$, $CH_3OC(O)Cl$ is more interesting because (1) both S_1 α C−Cl and C−O bond cleavages adiabatically correlate with their ground-state products and (2) both channels might exhibit nonadiabatic effects in the transition-state regions. But, it is not clear how important nonadiabatic effects in the transition-state regions are in the photodissociation dynamics of $CH_3OC(O)Cl$. Furthermore, contrast with the studies of the nascent photolytic product of $CH_3OC(O)Cl$, methoxycarbonyl radical, the exploration of $CH_3OC(O)Cl$ photodissociation dynamics has not gained much attention until 2007. Butler et al. studied the photodissociation dynamics of 193.3 nm irradiated $CH_3OC(O)Cl$, suggesting an excited-state electronic structure calculation in order to shed light on the details.[37,38] However, there is no theoretical work that concentrates on the photodissociation dynamics of $CH_3OC(O)Cl$ until now.

Quantum wavepacket method has played an important role in understanding the nuclear dynamics in reactive scattering, triatomic photodissociation dynamics, intramolecular energy redistribution, and the dynamics induced by pulsed laser excitation.[39−47] Quantum wavepacket method has also been extensively used to study nonadiabatic processes near conical intersections.[48−52] Therefore, we have good reasons to believe that the quantum wavepacket dynamics is helpful in shedding light on the nonadiabatic effects in transition-state regions on the bond-fission mechanism of Norrish type I reaction.

In this work, we have applied the multireference configuration interaction with single and double excitations (MR-CISD) and complete active space self-consistent field (CASSCF) methods to explore the pertinent S_1 and T_1 potential energy surfaces of $CH_3OC(O)Cl$ molecule. On the basis of the constructed diabatic S'_1 and S'_2 potential energy surfaces from the essential ab initio results of the adiabatic S_1 and S_2 states, the α bond-fission dynamics of $CH_3OC(O)Cl$ has been investigated using the time-dependent quantum wavepacket method. The results indicate that the S_1 α C−O bond cleavage is a typical adiabatic process in most excitation energy ranges, while, for the S_1 α C−Cl bond cleavage, it has strong nonadiabatic dynamics characteristics. This nonadiabatic bond-fission mechanism of Norrish type I reaction is uncovered for the first time and could also be helpful for understanding the similar excited-state, bond-cleavage reactions.

METHODS

Computational Details. We have optimized the stable structures (minima) and transition states (TSs) in the S_0 and S_1 electronic states with the state-specific CASSCF method. The nature of these critical points on the potential energy surfaces has also been checked by analyzing the harmonic vibrational frequencies. Specifically, at the TS structure, the vibrational mode with an imaginary frequency has an eigenvector that approximately corresponds to the reaction coordinate in the specific reaction, either C−Cl or C−C bond fission.

The active space selection in the CASSCF calculations requires some details. The active electrons (active orbitals) include π electrons of the C═O group (π and π^* orbitals), two pairs of lone electrons located at two O atoms (two n orbitals), and the involved σ electrons of the α C−Cl and α C−O bonds (two σ and σ^* orbitals), denoted as CASSCF(10,8). The cc-pVDZ and aug-cc-pVDZ basis sets are used in all calculations of this work. Unfortunately, the CASSCF calculations cannot provide sufficient correlation energy. Thus, the multireference configuration interaction with single- and double-excitations (MRCI-SD) method is used to refine the energetics of the CASSCF(10,8)/cc-pVDZ optimized structures with zero point energy (ZPE) correction at the CASSCF(10,8)/cc-pVDZ level. This MRCI-SD//CASSCF scheme can perform well for the photodissociation dynamics of carbonyl compounds.[22−28,34−36,53−55] In addition, the vertical excitation energy is calculated using the linear-response time-dependent density functional theory (TDDFT) method, the equation of motion coupled-cluster (EOM-CCSD) method, and the MRCI-SD method. All of the TDDFT and CASSCF calculations are carried out by using GAUSSIAN03, while the EOM-CCSD calculations make use of GAUSSIAN09. The MRCI-SD calculations are performed with MOLPRO-2006.[56−58]

Nonadiabatic Wavepacket Simulations. To solidify our understanding in the role of the off-diagonal potential coupling between the diabatic S'_1 and S'_2 states (S_1 and S_2 are used to indicate the adiabatic states) during the C−O and C−Cl bond fissions, we apply the variational method to obtain the predissociative vibrational states by solving the coupled Schrödinger equation

$$i\hbar\frac{\partial}{\partial t}\begin{pmatrix}\Psi_1\\ \Psi_2\end{pmatrix} = \left\{\begin{pmatrix}T & 0\\ 0 & T\end{pmatrix} + \begin{pmatrix}V_1 & V_{12}\\ V_{21} & V_2 - iV_o\end{pmatrix}\right\}\begin{pmatrix}\Psi_1\\ \Psi_2\end{pmatrix} \quad (2)$$

where the sine discrete variable representation (DVR) technique and the optical potential method are used.[59−62] V_1 and V_2 are the diabatic potential energy curves of the S'_1 and S'_2 electronic states as a function of the C−O or C−Cl bond length, and V_{12} is the off-diagonal potential coupling between the S'_1 and S'_2 electronic states. iV_o is the imaginary optical potential applied at the ending range of the DVR grid points.[61] Additionally, we also carry out the time-dependent wavepacket calculations by solving eq 2 in an explicit time-dependent form. The second-order split operator method, which is written as[63]

$$\exp(-iH\Delta_t) = \exp(-iV\Delta_t/2)\exp(-iT\Delta_t)\exp(-iV\Delta_t/2) \quad (3)$$

is applied to propagate the initial wavepacket in the coupled S'_1 and S'_2 electronic states. In the wavepacket calculations, the fast sine transformation technique is used to switch the propagated wave function between the DVR and the kinetic energy representations.[60,64] More details of the algorithms can be found in the recent literature.[14,43,64]

Table 1. Main Bond Lengths (Å) of the CASSCF(10,8)/cc-pVDZ Optimized Structures and Their MRCI-SD/cc-pVDZ Refined Relative Energies with (without) the CASSCF(10,8)/cc-pVDZ Calculated ZPE Correction (kcal/mol)

	C1−O2	C1−O3	C1−Cl5	O3−C4	energies
S0-MIN	1.193	1.312	1.766	1.425	00.00 (00.00)
S1-MIN	1.380	1.322	1.807	1.425	102.2 (104.9)
S1−O−TS	1.228	1.667	1.753	1.409	111.9 (120.5)
S1−Cl−TS	1.291	1.303	2.073	1.429	103.7 (108.6)

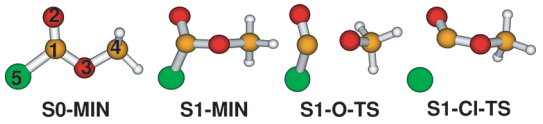

Figure 1. CASSCF(10,8)/cc-pVDZ optimized geometry structures with the labeled atoms (1 and 4, carbon; 2 and 3, oxygen; 5, chlorine; others, hydrogen).

RESULTS

The structural parameters of the CASSCF(10,8)/cc-pVDZ optimized structures are tabulated in Table 1 with the MRCI-SD/cc-pVDZ refined single-point energies. Each structure is given one symbol for the discussion below, as shown in Figure 1. Specifically, S1-MIN, S1−O−TS, and S1−Cl−TS are the equilibrium structure, and the transition states for the C−O and C−Cl bond cleavages in the S_1 state, respectively. Furthermore, $CH_3OC(O)Cl$ has two main conformers with respect to the C1−O3 bond, namely, TRANS and CIS. On the ground state, CIS (referred to as S0-MIN hereinafter) is more stable than TRANS. More details about the S_0 conformers can be found in the Supporting Information.

Transition Energies. The transition energies of $CH_3OC(O)Cl$ in the Franck−Condon region is very useful for understanding both the electronic structures of the initially populated excited states and their subsequent decay dynamics. By means of the CASSCF(10,8)/cc-pVDZ, MRCI-SD/cc-pVDZ, EOM-CCSD/aug-cc-pVDZ methods, and the TDDFT/cc-pVDZ method with the B3LYP exchange-correlation functional, we have calculated the vertical transition energies of the first electronically excited singlet state (S_1), which are listed in Table 2. It is clear that the transition energy to the S_1 state, predicted by the different methods, is consistent. This electronic transition, based on the MO population analysis, is assigned to be $n \rightarrow \pi^*$ excitation, where n is the lone-pair orbital of the O2 atom; π and π^* are the bonding and antibonding MOs of the C1═O2 group.

Minimum-Energy Structure in the S_1 State. The geometric structure of $CH_3OC(O)Cl$ in the S_1 state was optimized at the CASSCF(10,8)/cc-pVDZ level. The obtained structure, referred to as S1-MIN hereafter, is schematically shown in Figure 1, and the selected bond parameters are listed in Table 1. As compared with the S0-MIN structure, the largest changes in the S1-MIN structure are associated with the C1−O2 bond length and the Cl5−C1−O2−C3 dihedral angle. The C1−O2 bond is elongated from 1.193 Å in S0-MIN to 1.380 Å in S1-MIN, while the Cl5−C1−O2−C3 dihedral angle is decreased by ~50° from S0-MIN to S1-MIN. The CASSCF(10,8)/cc-pVDZ calculated wave function reveals that the S1-MIN state originates mainly from the

Table 2. Transition Energies (kcal/mol) of CIS in the Franck−Condon Region with the Different ab Initio Electronic Structure Methods

	S_1		S_1
CASSCF(10,8)	150.1	TD-B3LYP	142.6
MRCI-SD	151.4	EOM-CCSD	149.3

$n \rightarrow \pi^*$ excitation localized on the carbonyl group. One-electron excitation from n to π^* orbitals leads to a partial breaking of the C1−O2 π bond, which is the reason why the C1−O2 bond is significantly elongated in S1-MIN with respect to that in the S1-MIN structure. In addition, the $n \rightarrow \pi^*$ excitation results in a rehybridization of orbitals on the carbonyl carbon atom from sp^2 of S0-MIN to sp^3 of S1-MIN, causing a large change in the Cl5−C1−O2−C3 dihedral angle from the S0-MIN planar structure to the S1-MIN pyramidal structure. The adiabatic excitation energy corresponding to the energy difference between S1-MIN and S0-MIN is predicted to be 102.2 kcal/mol at the MRCI-SD/cc-pVDZ//CASSCF(10,8)/cc-pVDZ level with the CASSCF(10,8)/cc-pVDZ calculated ZPE correction.

Transition States in the S_1 State. Determining transition-state structures and their barriers is very important for understanding mechanisms of chemical reactions and calculating the corresponding rate constants quantitatively. In the S_1 state, we have obtained the transition states responsible for the C−O and C−Cl bond fissions, which are referred to as S1−O−TS and S1−Cl−TS, as shown in Figure 1. The subsequent frequency analyses of S1−O−TS and S1−Cl−TS ensure that they are the TSs of the S_1 C−O and C−Cl bond cleavages. In S1−O−TS, the C1−O3 bond is about to dissociate; its bond length is 1.667 Å at the CASSCF(10,8)/cc-pVDZ level, which is longer than that in S1-MIN by about 0.345 Å. The potential energy of S1−O−TS relative to S1-MIN, namely, the barrier of the C−O bond cleavage, is predicted to be 9.7 kcal/mol at the MRCI-SD/cc-pVDZ//CASSCF(10,8)/cc-pVDZ level with the CASSCF(10,8)/cc-pVDZ calculated ZPE correction. Without the ZPE correction, it is 15.6 kcal/mol, as shown in Table 1. This difference is originated from the fact that the ZPE of S1−O−TS is smaller than that of S1-MIN due to an imaginary frequency in the former one. Similarly, in S1−Cl−TS, the C1−Cl5 bond length is 2.073 Å at the CASSCF(10,8)/cc-pVDZ level, indicating that this bond will be dissociating. The barrier of the C−Cl bond fission is calculated to be 1.5 kcal/mol at the MRCI-SD/cc-pVDZ//CASSCF(10,8)/cc-pVDZ level with the CASSCF(10,8)/cc-pVDZ calculated ZPE correction, and to be 3.7 kcal/mol without this correction. The structural parameters and the refined single-point energies of S1−O−TS and S1−Cl−TS are summarized in Table 1.

Energy Gaps between the S_2 and S_1 States in the Transition-State Regions. As can be seen from Table 1, the C1−Cl5 bond is significantly elongated (0.041 Å) from S0-MIN to S1-MIN. The reason for this comes from a little contribution of the $n_{Cl}\sigma^*_{C-Cl}$ excited configuration to the electronic wave function of the S1-MIN structure. The contribution of the $n_{Cl}\sigma^*_{C-Cl}$ configuration becomes very important in the S1−Cl−TS region with its weight of about 40% in the wave function. Actually, the transition state of S1−Cl−TS results from an avoided interaction between the S_1 ($n_{Cl}\sigma^*_{C-Cl}$) and S_2 ($\sigma_{Cl}\sigma^*_{C-Cl}$) states. Also, the transition state of S1−O−TS comes from the avoided interaction between the S_1 and S_2 states. But the $\sigma_{C-O}\sigma^*_{C-O}$

Table 3. Calculated Energy Gaps (kcal/mol) of the Transition-State Regions for the C−Cl and C−O Bond Fissions

	CASSCF(10,8)/cc-pVDZ	MRCI-SD/cc-pVDZ
E12−Cl−TS	9.6	12.5
E12−O−TS	32.7	32.3

excited configuration has the main contribution to the S_2 wave function in the S1−O−TS region. To understand the relative strength of the avoided interaction in the two transition-state regions, we calculate the energy gaps between the S_2 and S_1 states in the transition-state regions and the obtained results are listed Table 3. The energy gap between the S_1 and S_2 states in the vicinity of S1−Cl−TS is predicted to be 9.6 kcal/mol at the CASSCF(10,8)/cc-pVDZ level and 12.5 kcal/mol at the MRCI-SD//CASSCF(10,8)/cc-pVDZ level. In close proximity to S1−O−TS, however, the energy gap is increased to 32.7 and 32.3 kcal/mol at the CASSCF(10,8)/cc-pVDZ and the MRCI-SD//CASSCF(10,8)/cc-pVDZ levels, respectively. The calculated energy gaps predict that the avoided interaction is much weaker in the S1−Cl−TS region than in the S1−O−TS region, which gives us a hint that the S_1 C−Cl fission may be a nonadiabatic process.

To identify whether the involved S_1 fission process (C−O or C−Cl bond cleavages) is nonadiabatic, we calculate the energy gaps between the S_2 and S_1 states in the transition-state regions, as shown in Table 3. This is similar to the earlier work of Butler et al.; however, studying Norrish type I reaction with this approach is the first time.[2] In this work, we have predicted that the energy gap between S_2 and S_1 in the vicinity of S1−Cl−TS is 9.6 kcal/mol at the CASSCF(10,8)/cc-pVDZ level and 12.5 kcal/mol at the MRCI-SD/cc-pVDZ//CASSCF(10,8)/cc-pVDZ level; in close proximity to S1−O−TS, however, the energy gap increases to 32.7 and 32.3 kcal/mol at the CASSCF-(10,8)/cc-pVDZ level and the MRCI-SD/cc-pVDZ//CASSCF-(10,8)/cc-pVDZ levels, respectively.

Construction of the Simplified Mutistate Potential Energy Surfaces. Before the nonadiabatic wavepacket calculations, we need first set up the relevant potential energy curves. In the current work, we only focus on the nonadiabatic recrossing effect in the transition-state region on the dynamics of the C−O or C−Cl bond fission; thus, the simplified, multistate, one-dimensional diabatic potential energy curves are expected to be able to unravel this effect to some extent. The multistate one-dimensional potential energy curves describing the C−O bond fragmentation are constructed as follows. The one-dimensional Morse potential with a vibrational frequency of 1381 cm^{-1} corresponding to the C═O stretching vibrational mode in the adiabatic S_1 state, which is calculated by the CASSCF(10,8)/cc-pVDZ method, is used to describe the diabatic bound potential energy curve of the C−O bond in the diabatic S'_1 state, while the repulsive diabatic potential energy curve describing the C−O cleavage in the diabatic S'_2 state is described by an exponential function, whose asymptotic energy is higher than the minimum of the S'_1 Morse potential of the C−O bond, by 4.3 kcal/mol (Figure 5). The off-diagonal potential coupling, V_{12} in eq 2, is assumed to be Gaussian shape, with the width of 1.0 bohr and the height of 32.3 kcal/mol, which is the energy gap between the adiabatic S_1 and S_2 states in the transition-state region, as shown in Figure 5. The Gaussian shape is centered at the crossing point of the diabatic S'_1 and S'_2 potential curves. The slope of the exponential function of the diabatic S'_2 state and the dissociation energy of the Morse potential of the diabatic S'_1 state are optimized so that the barrier height of 15.6 kcal/mol of the adiabatic S_1 state and the imaginary vibrational frequency at the transition state of the C−O bond fission of the ab initio results are reproduced. Similarly, the simplified multistate one-dimensional potential energy curves for the C−Cl bond fission are constructed. The resulted potential energy curves in the diabatic and adiabatic representations are shown in Figure 2. One should be aware that even these simplified one-dimensional potential curves are functions of only one active bond distance; the other inactive bonds effectively change along with the variation of the active bond distance to follow the reaction path.

Time-Independent Quantum Calculations. Figure 2 illustrates that the S_1 adiabatic potential energy curve of the C−O bond fission has a shallow well, and the well of the S_1 C−Cl adiabatic potential energy curve is much shallower and has relatively lower asymptotic energy than those of the C−O bond, as indicated by eq 2. As a result, we can expect there are several long-lifetime vibrational states for the coupled potential energy curve of the C−O bond—the lowest four vibrational states, as shown in the right panel of Figure 3. However, only the lowest two vibrational states for the C−Cl coupled potential energy curves have long lifetimes, as shown in Figure 3, which are the vibrational states in which the quantum number is less than 2.

For the vibrational states whose energies are around the crossing point, they all have very short lifetimes. The wave functions of $v = 3$ for the C−Cl bond and $v = 5$ for the C−O bond, shown in Figure 2, are two typical vibrational states. However, at the higher vibrational energies, there are many vibrational states for the C−Cl coupled states, which have longer lifetimes than those for the C−O coupled states. Typical vibrational wave functions, $v = 9$ for the C−Cl bond and $v = 14$ for the C−O bond, are shown in Figure 3. This reflects the small energy gap in S1−Cl−TS for the C−Cl bond fission (12.5 kcal/mol calculated at the MRCI-SD/cc-pVDZ level shown in Table 3) between the adiabatic S_1 and S_2 states and reflects the weak off-diagonal potential coupling V_{12} between the diabatic S'_1 and S'_2 potential curves. The weak coupling of the S'_1 and S'_2 potential curves leads to inefficient population transfer between them, which results in the observation of the S_1 bound state characteristics, in contrast with those for the C−O bond.

Time-Dependent Quantum Wavepacket Calculations. To obtain an overall comparative picture describing the C−O and C−Cl bond cleavages in the coupled diabatic S'_2 and S'_1 states, we have carried out time-dependent wavepacket calculations to study the dissociation processes from the state excited by an ultrashort laser pulse and to calculate the absorption spectra. The characteristics of such a whole energy range spectrum provides us a clear overall picture of the lifetimes of the vibrational states.

The initial excited state on the diabatic S'_1 potential energy curve is created by a vertical excitation from the lowest vibrational state of the S_0 state by a laser pulse of infinite short width. The Duschinsky rotation effect during the excitation is ignored, which should be unimportant to the issues investigated here.[65] The potential energy curves of the C−O and C−Cl bonds of the S_0 state have the Morse forms, whose vibrational frequencies are the same as those of ab initio calculated C−O and C−Cl vibrational modes. The relative displacements of the minima of the C−O and C−Cl bonds are also approximated, which only influence the central position of the overall spectra. However, it is noted that in a practical experiment the laser pulse has specific

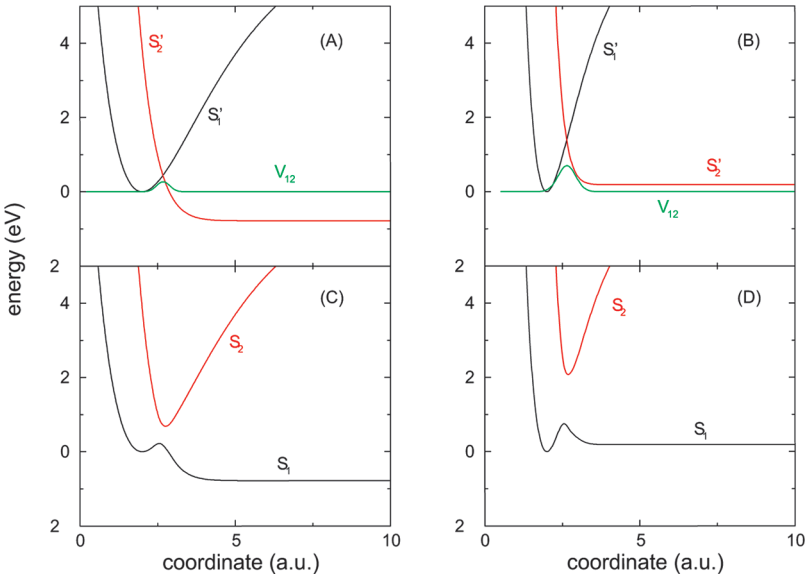

Figure 2. Diabatic (panel A) and adiabatic (panel C) potential energy curves with respect to the effective C−Cl bond distance and the diabatic (panel B) and adiabatic (panel D) potential energy curves with respect to the effective C−O bond distance of $CH_3OC(O)Cl$ in the S_1 and S_2 states. The curves are constructed using the results from the MRCI-SD/cc-pVDZ//CASSCF(10,8)/cc-pVDZ method.

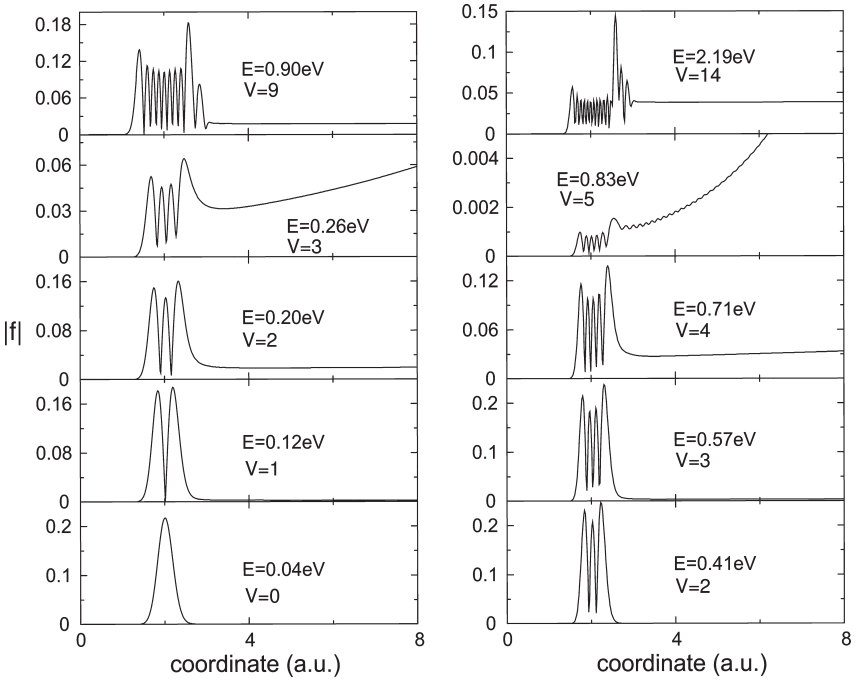

Figure 3. Vibrational states and quantum numbers of the indicated eigenenergies of the adiabatic S_1 and S_2 states for the C−Cl (left panels) and C−O (right panels) bonds calculated using the DVR and the optical potential methods.

time duration and wavelength. In that case only part of the overall spectra shown in Figure 4 are relevant, whose adiabaticity/nonadiabaticity may vary greatly.

The absorption spectra calculated by the autocorrelation function and the fragment accumulations as a function of time calculated by the flux formalism are shown in Figure 4.[41,66,67] It is seen from the right panels that after the excitation, the C−O bond breaks very quickly and nearly completely, about 7 fs along this C−O vibrational mode. This is ascribed to the short vibrational periodic time of the C−O vibrational mode and large off-diagonal potential coupling V_{12} between the diabatic S'_1 and S'_2 states. This means that when the S_1 system moves across S1−O−TS, the system does not encounter the adiabatic S_2 potential energy surface and proceeds adiabatically with dissociation into the products. However, due to relatively long vibrational periodic time of the C−Cl bond, the excited-state population on the diabatic S'_1 potential energy curve runs into the diabatic S'_2 state relatively slow, about 17 fs. And after this

dx.doi.org/10.1021/jp2053025 |J. Phys. Chem. A 2011, 115, 10146–10153

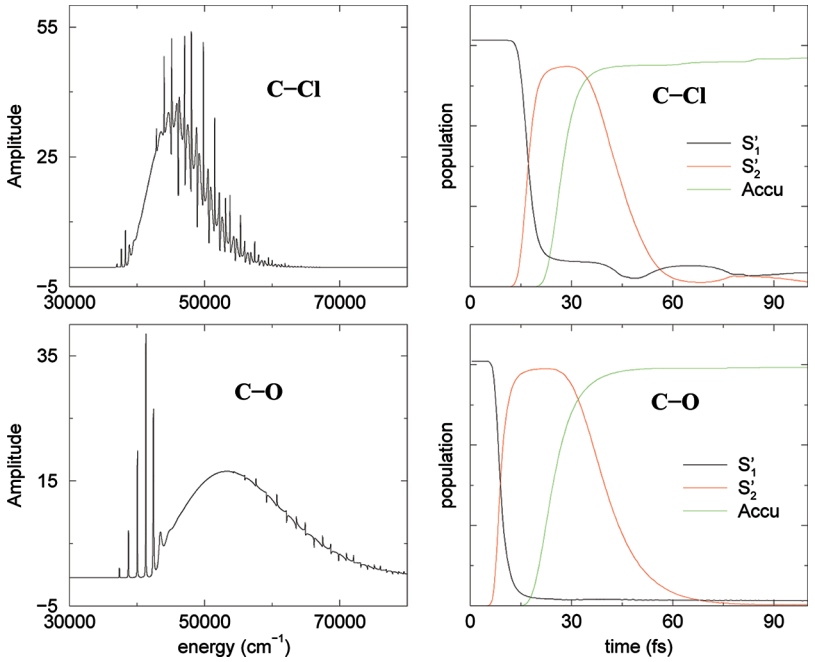

Figure 4. Absorption spectra of the coupled models for both the C−O and the C−Cl bonds are plotted in the left panels, and the time-dependent populations on the diabatic S'_1 and S'_2 states are shown in the right panels. The lines indicated by the "Acc" are the accumulated fragment products collected at the asymptotic regions.

time, a small part of the S'_1 population oscillates, instead of approaching zero. This means a large part of the population proceeds to product via an adiabatic way, determined by the energy of the initial wavepacket which is around the crossing point of the diabatic states S'_1 and S'_2. Only a small part of the initial population has energy apart from that crossing point, which has a longer lifetime and dissociates slowly into product. At the same time, it exchanges between the diabatic S'_1 and S'_2 states, originating from the small off-diagonal potential coupling V_{12} in the transition-state region of the C−Cl bond fission, which leads to the oscillation at a later time.

From the results in the left panels of Figure 4, we see that the absorption spectrum of the C−O bond is quite smooth without sharp peaks except the lowest several ones (a few states with relative longer lifetime due to the efficient presence of a well in the S_2 adiabatic potential energy surface). However that of the coupled state for the C−Cl bond has many sharp peaks except in the energy range around the crossing points of the two diabatic potential energy curves S'_1 and S'_2. This means that in most excitation energy ranges, the vibrational states of the C−O bond from the coupled S'_1 and S'_2 states have much shorter lifetime than those of the C−Cl bond. Due to the small potential coupling V_{12} in the S1−Cl−TS region, the population transfer between the S'_1 and S'_2 states occurs less efficiently than those for the C−O bond where there is a large potential coupling in S1−O−TS between the S'_1 and S'_2 states. Therefore, the population initially staying at the diabatic S'_1 state dissociates to the product along S_1 curves much easier for the C−O bond than for the C−Cl bond, especially at the excitation energy range higher than the crossing point of the S'_1 and S'_2 states. At the crossing point energy, the dissociation processes of the C−O and C−Cl bond is more similar, which also explains the similarity of the time dependence of the populations in the right panels in Figure 4. If we make the initial excited wavepacket have higher energy, the oscillations in the residual population would be sharper for the C−Cl bond. However, that for the C−O bond would be roughly unchanged.

From the discussion above, we may expect that for the excitation energy around diabatic state crossing points, the branch ratio for the bond breakage of C−O and C−Cl may be determined mostly by the Franck−Condon factor between the S_0 state and the S_1 or S'_1 state. However, when we have higher excitation energy, due to a longer lifetime of the C−Cl bond, the breakage of the C−O bond may be relatively more efficient.

Finally, since the simplified multistate potential energy surfaces for the C−O and C−Cl bond fissions are used, it is hence not expected that the results shown in Figure 4 are rigorously accurate; however, the uncertainty should not harm our study on the nonadiabatic effect in the transition-state region on the bond-fission mechanism and we may gain a greater picture from such time-dependent wavepacket study.

DISCUSSIONS

Adiabatic S_1 C−O Bond Fission. Figure 5 illustrates the relevant potential energy profiles of the C1−O3 bond cleavage. This bond cleavage in the S_1 state can be considered as an adiabatic process due to the large energy gap between the S_2 and S_1 states in the vicinity of S1−O−TS. This energy gap is predicted to be 32.3 kcal/mol at the MRCI-SD/cc-pVDZ//CASSCF(10,8)/cc-pVDZ level, very close to 32.7 kcal/mol calculated by the CASSCF(10,8)/cc-pVDZ method (Table 3). After $CH_3OC(O)Cl(S_0)$ is excited to the S_1 state with the low excitation energy, about 151.4 kcal/mol (Table 2) at the MRCI-SD/cc-pVDZ//CASSCF(10,8)/cc-pVDZ method, the kinetic energy of the system will rapidly increase in the S_1 relaxation process, in conjunction with the decrease of the potential energy. The potential energy of the S_2 state in the vicinity of S1−O−TS is a little higher than the total energy of $CH_3OC(O)Cl(S_1)$, 152.8

dx.doi.org/10.1021/jp2053025 |J. Phys. Chem. A 2011, 115, 10146–10153

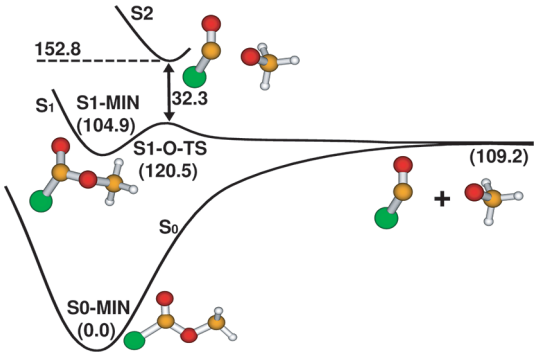

Figure 5. Schematic potential energy profiles for the α -C−O bond cleavage of CH3OC(O)Cl in the S_0 and S_1 states. The relative potential energies (kcal/mol) are calculated with the MRCI-SD/cc-pVDZ//CASSCF(10,8)/cc-pVDZ method.

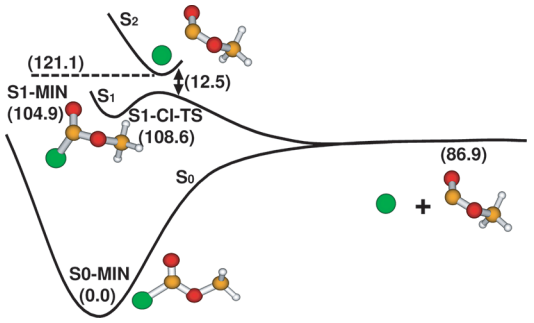

Figure 6. Schematic potential energy profiles for the α C−Cl bond cleavage of CH3OC(O)Cl in the S_0 and S_1 states. The relative energies (kcal/mol) are calculated with the MRCI-SD/cc-pVDZ//CASSCF-(10,8)/cc-pVDZ method.

kcal/mol versus 151.4 kcal/mol; thus, when the S_1 system moves across S1−O−TS, it will not encounter the S_2 state due to the large energy gap in the transition-state region and will adiabatically dissociate into the ground-state products of the α C−O bond fission. Usually the larger the energy gap in the transition state is, the weaker the nonadiabatic effect is. In such case, the nonadiabatic transitions near the transition state become inefficient due to the large energy gap. Furthermore, the above wavepacket calculations also to some extent demonstrate the nonadiabatic effect is negligible in S1−O−TS. Hence, this S_1 C−O bond fission with low excitation energy can be considered as an adiabatic process.

Nonadiabatic S_1 C−Cl Bond Fission. In contrast to the C−O bond fission, we may expect that the C−Cl bond cleavage in the S_1 state is a nonadiabatic process in most excitation energy ranges due to the small energy gap between the S_1 and S_2 states around S1−Cl−TS. This energy gap is predicted to be 9.6 kcal/mol at the CASSCF(10,8)/cc-pVDZ level and 12.5 kcal/mol at the MR-CI-SD/cc-pVDZ//CASSCF(10,8)/cc-pVDZ level. In the vicinity of S1−Cl−TS, the potential energy of the S_2 state is much lower than the total energy of $CH_3OC(O)Cl(S_1)$, 121.1 kcal/mol versus 151.4 kcal/mol. Usually the smaller the energy gap is, the stronger the nonadiabatic effect is. If the energy gap between the S_2 and S_1 states in the transition state is small, the S_1 system with low excitation energy must encounter the S_2 potential energy surface when the system moves across the transition state. In such case, the bond fission cannot be regarded as an adiabatic process because the nonadiabatic transitions near the transition state can easily occur due to the small energy gap. When $CH_3OC(O)Cl(S_1)$ molecule approaches the transition-state region of the C−Cl bond cleavage, namely, S1−Cl−TS, the nonadiabatic transitions between S_1 and S_2 will take place as a result of the small energy gap. Thereby, this C−Cl bond fission cannot be fully treated as an adiabatic process; it should exhibit strong nonadiabatic bond-fission characteristics, which is also observed in the above wavepacket calculations.

Adiabatic and Nonadiabatic Bond Cleavages in Norrish Type I Reaction. In this work, we have presented a striking example of breakdown of the adiabatic bond-fission picture in the S_1 Norrish type I reactions of $CH_3OC(O)Cl$. In terms of the present calculations, there are two main dissociation channels for $CH_3OC(O)Cl$ in the S_1 state: the adiabatic α C−O and the nonadiabatic α C−Cl bond cleavages, as shown in Figure 5 and Figure 6. Due to a large energy gap between the S_1 and S_2 states in S1−O−TS, $CH_3OC(O)Cl(S_1)$ cannot encounter the S_2 potential energy surface when the S_1 system moves across the transition state, meaning that the α C−O bond cleavage adiabatically dissociates in the S_1 state. Conversely, the S_1 α C−Cl bond cleavage fissions with more nonadiabatic characteristics as a result of a small energy gap between the S_2 and S_1 states and the low energy of the S_2 state in S1−Cl−TS.

This nonadiabatic bond-fission picture will provide new insights into Norrish type I reactions, complementary to the previous adiabatic picture.[22−28] In addition, by using the time-independent and -dependent wavepacket dynamics simulations, it has been qualitatively demonstrated that the inclusion of the nonadiabatic effect in the transition-state region is significant for understanding the mechanistic photodissociation of $CH_3OC(O)Cl$ both correctly and accurately.

CONCLUSIONS

In this work, the mechanisms of the α bond fissions of $CH_3OC(O)Cl$ in the S_1 state have been studied on the basis of the obtained S_1 and S_0 potential energy surfaces, which are calculated by means of the MRCI-SD and the CASSCF methods with the cc-pVDZ basis set. In terms of the energy gaps between the S_1 and S_2 states in the transition-state regions of the α bond fissions and the relevant potential energy surfaces of the S_1 and S_0 electronic states, we suggest that the S_1 α C−O bond cleavage can be considered as an adiabatic dissociation process, while the nonadiabatic effect probably plays an important role in the S_1 α C−Cl bond cleavage. Further evidence comes from the time-independent and -dependent quantum wavepacket simulations, which to some extent show that the nonadiabatic effect in the transition-state region is very important for correctly understanding the bond-fission mechanism of Norrish type I reaction. This nonadiabatic bond-fission picture for Norrish type I reaction is totally different from the previous one, where the bond fissions are discussed by using an adiabatic multidimensional potential energy surface.[24,34−36,53] Furthermore, it is also expected that this nonadiabatic bond-fission picture is common to Norrish type I reactions of a wide variety of ketones. Finally, evaluating the branching ratio itself is outside the scope of this study and would be an interesting target for future calculations.

ASSOCIATED CONTENT

Supporting Information. Figure showing the optimized conformers on the ground state. This information is available free of charge via the Internet at http://pubs.acs.org.

AUTHOR INFORMATION

Corresponding Author
*E-mail: fangwh@bnu.edu.cn.

ACKNOWLEDGMENT

W.F. thanks the NSFC (Grant No. 20720102038) and the Major State Basic Research Development Programs (Grant No. 2004CB719903).

REFERENCES

(1) Domcke, W.; Yarkony, D. R.; Köppel, H. *Conical Intersections: Electronic Structure, Dynamics & Spectroscopy*; World Scientific: Singapore, 2004.
(2) Butler, L. J. *Annu. Rev. Phys. Chem.* **1998**, *49*, 125–171.
(3) Kash, P. W.; Waschewsky, G. C. G.; Butler, L. J.; Francl, M. M. *J. Chem. Phys.* **1993**, *99*, No. 4479.
(4) Worth, G. A.; Cederbaum, L. S. *Annu. Rev. Phys. Chem.* **2004**, *55*, 127–158.
(5) Yarkony, D. R. *J. Phys. Chem.* **1996**, *100*, 18612–18628.
(6) Chen, L.; Ren, Z. F.; Wang, X. G.; Dong, W. R.; Dai, D. X.; Wang, X. Y.; Zhang, D. H.; Yang, X. M.; Sheng, L. S.; Li, G. L.; Werner, H. J.; Lique, F.; Alexander, M. H. *Science* **2007**, *317*, 1061–1064.
(7) Valero, R.; Truhlar, D. G. *J. Chem. Phys.* **2006**, *125*, No. 194305.
(8) Krishna, V. *Phys. Rev. Lett.* **2009**, *102*, No. 053002.
(9) Takatsuka, K. *Int. J. Quantum Chem.* **2009**, *109*, 2131–2142.
(10) Bushmaker, A. W.; Deshpande, W.; Hsieh, S.; Bockrath, M. W.; Cronin, S. B. *Nano Lett.* **2009**, *9*, 607–611.
(11) Doltsinis, N. L.; Marx, D. *Phys. Rev. Lett.* **2002**, *88*, No. 166402.
(12) Craig, C. F.; Duncan, W. R.; Prezhdo, O. V. *Phys. Rev. Lett.* **2005**, *95*, No. 163001.
(13) Yarkony, D. R. *Rev. Mod. Phys.* **1996**, *68*, 985.
(14) Sun, Z. G.; Zhang, D. H.; Alexander, M. *J. Chem. Phys.* **2010**, *132*, No. 034308.
(15) Norrish, R. G. W.; Bamford, C. H. *Nature* **1936**, *138*, 1016–1016.
(16) Norrish, R. G. W.; Bamford, C. H. *Nature* **1937**, *140*, 195–196.
(17) Laue, T.; Plagens, A. *Named Organic Reactions*; John Wiley & Sons: New York, 2005.
(18) March, J. *Advanced Organic Chemistry*; Wiley-Interscience: New York, 1992.
(19) De Feyter, S.; Diau, E. W. G.; Zewail, A. H. *Angew. Chem., Int. Ed.* **2000**, *112*, 266–269.
(20) Diau, E. W. G.; Kotting, C.; Zewail, A. H. *ChemPhysChem* **2001**, *2*, 273–293.
(21) Diau, E. W. G.; Kotting, C.; Zewail, A. H. *ChemPhysChem* **2001**, *2*, 294–309.
(22) Xiao, H. Y.; Liu, Y. J.; Fang, W. H. *J. Chem. Phys.* **2007**, *127*, No. 244313.
(23) Cui, G. L.; Zhang, F.; Fang, W. H. *J. Chem. Phys.* **2010**, *132*, No. 034306.
(24) Fang, W. H. *Acc. Chem. Res.* **2008**, *41*, 452–457.
(25) He, H. Y.; Fang, W. H. *J. Am. Chem. Soc.* **2003**, *125*, 16139–16147.
(26) Chen, X. B.; Fang, W. H.; Fang, D. C. *J. Am. Chem. Soc.* **2003**, *125*, 9689–9698.
(27) Chen, S. L.; Fang, W. H. *J. Chem. Phys.* **2009**, *131*, No. 054306.
(28) Ding, W. J.; Fang, W. H.; Liu, R. Z.; Fang, D. C. *J. Chem. Phys.* **2002**, *117*, No. 8745.
(29) Bacchus-Montabonel, M.; Vaeck, N.; Lasorne, B.; Desouter-Lecomte, M. *Chem. Phys. Lett.* **2003**, *374*, 307–313.
(30) Lasorne, B.; Bacchus-Montabonel, M.; Vaeck, N.; Desouter-Lecomte, M. *J. Chem. Phys.* **2004**, *120*, No. 1271.
(31) Lasorne, B.; Bacchus-Montabonel, M.; Vaeck, N.; Desouter-Lecomte, M. *Int. J. Quantum Chem.* **2006**, *106*, 670–675.
(32) Zhang, F.; Ding, W. J.; Fang, W. H. *J. Chem. Phys.* **2006**, *125*, No. 184305.
(33) Lee, S. H. *J. Chem. Phys.* **2008**, *129*, No. 194304.
(34) Cui, G. L.; Li, Q. S.; Zhang, F.; Fang, W. H.; Yu, J. G. *J. Phys. Chem. A* **2006**, *110*, 11839–11846.
(35) Chen, S. L.; Fang, W. H. *J. Phys. Chem. A* **2007**, *111*, 9355–9361.
(36) Fang, W. H. *J. Am. Chem. Soc.* **1999**, *121*, 8376–8384.
(37) Bell, M. J.; Lau, K. C.; Krisch, M. J.; Bennett, D. I. G.; Butler, L. J.; Weinhold, F. *J. Phys. Chem. A* **2007**, *111*, 1762–1770.
(38) McCunn, L. R.; Lau, K. C.; Krisch, M. J.; Butler, L. J.; Tsung, J. W.; Lin, J. J. *J. Phys. Chem. A* **2006**, *110*, 1625–1634.
(39) Tannor, D. In *Encyclopedia of Chemical Physics and Physical Chemistry*; Moore, J., Spencer, N., Eds.; Institute of Physics: London, 2001; p A1.6.
(40) McCullough, E. A.; Wyatt, R. E. *J. Chem. Phys.* **1971**, *54*, No. 3578.
(41) Zhang, D. H.; Zhang, J. Z. H. *J. Chem. Phys.* **1993**, *99*, No. 5615.
(42) Qiu, M. H.; Ren, Z. F.; Che, L.; Dai, D. X.; Harich, S. A.; Wang, X. Y.; Yang, X. M.; Xu, C. X.; Xie, D. Q.; Gustafsson, M.; Skodje, R. T.; G., S. Z.; Zhang, D. H. *Science* **2006**, *311*, 1440–1443.
(43) Sun, Z. G.; Liu, L.; Lin, S. Y.; Schinke, R.; Guo, H.; Zhang, D. H. *Proc. Natl. Acad. Sci. U. S. A.* **2010**, *107*, 555–558.
(44) Butler, L. J.; Neumark, D. M. *J. Chem. Phys.* **1996**, *100*, No. 12801.
(45) Hairer, E.; Lubich, C.; Wanner, G. *Geometric Numerical Integration: Structure-Preserving Algorithms for Ordinary Differential Equations*; Springer: Dordrecht, The Netherlands, 2006.
(46) Schinke, R. *Photodissociation Dynamics Spectroscopy and Fragmentation of Small Polyatomic Molecules*; Cambridge University Press: New York, 1993.
(47) Fair, J. R.; Schaefer, D.; Kosloff, R.; Nesbitt, D. J. *J. Chem. Phys.* **2001**, *116*, No. 1406.
(48) Seel, M.; Domcke, W. *Chem. Phys.* **1991**, *151*, 59–72.
(49) Seel, M.; Domcke, W. *J. Chem. Phys.* **1991**, *95*, No. 7806.
(50) Seidner, L.; Domcke, W. *Chem. Phys.* **1994**, *186*, 27–40.
(51) Lan, Z. G.; Domcke, W.; Vallet, V.; Sobolewski, A.; Mahapatra, S. *J. Chem. Phys.* **2005**, *122*, No. 224315.
(52) Vallet, V.; Lan, Z.; Mahapatra, S.; Sobolewski, A.; Domcke, W. *J. Chem. Phys.* **2005**, *123*, No. 144307.
(53) Chen, S. L.; Fang, W. H. *J. Phys. Chem. A* **2006**, *110*, 944–950.
(54) Liu, D.; Fang, W. H.; Fu, X. Y. *Chem. Phys. Lett.* **2000**, *325*, 86–92.
(55) Lin, L.; Zhang, F.; Ding, W. J.; Fang, W. H.; Liu, R. Z. *J. Phys. Chem. A* **2005**, *109*, 554–561.
(56) Frisch, M. J.; et al. *Gaussian 03*, Revision D.01; Gaussian: Wallingford, CT, 2004.
(57) Frisch, M. J.; et al. *Gaussian09*, Revision A.02; Gaussian, Wallingford, CT, 2009.
(58) Werner, H. J.; et al. *MOLPRO*, version 2006.6, a package of ab initio programs. 2006; see http://www.molpro.net.
(59) Choi, S. E.; Light, J. C. *J. Chem. Phys.* **1990**, *92*, No. 2129.
(60) Colbert, D. T.; Miller, W. H. *J. Chem. Phys.* **1992**, *96*, No. 1982.
(61) Jolicard, G.; Leforestier, C.; Austin, E. J. *J. Chem. Phys.* **1988**, *88*, No. 1026.
(62) Light, J. C.; Carrington, T. *Adv. Chem. Phys.* **2000**, *114*, 263–310.
(63) Feit, M. D.; Fleck, J. A., Jr.; Steiger, A. *J. Comput. Phys.* **1982**, *47*, 412–433.
(64) Kosloff, R. *J. Phys. Chem.* **1988**, *92*, 2087–2100.
(65) Duschinsky, F. *Acta Physicochim. URSS* **1937**, *7*, 551–566.
(66) Heller, E. J. *J. Chem. Phys.* **1978**, *68*, No. 3891.
(67) Heller, E. J. *Acc. Chem. Res.* **1981**, *14*, 368–375.